PLCG2 as a Risk Factor for Alzheimer's Disease.

Andy P. Tsai[1], Chuanpeng Dong[2], Christoph Preuss[3], Miguel Moutinho[1], Peter Bor-Chian Lin[1], Nicole Hajicek[4], John Sondek[4], Stephanie J. Bissel[1,6], Adrian L. Oblak[1,7], Gregory W. Carter[3], Yunlong Liu[2], Gary E. Landreth[1,5], Bruce T. Lamb[1,6], Kwangsik Nho[7*]

[1.] Stark Neurosciences Research Institute, IUSM, Indianapolis, IN, USA.

[2.] Department of Medical and Molecular Genetics, Center for Computational Biology and Bioinformatics, IUSM, Indianapolis, IN, USA.

[3.] The Jackson Laboratory, Bar Harbor, ME, USA

[4.] Department of Pharmacology, The University of North Carolina at Chapel Hill, Chapel Hill, NC, USA

[5.] Department of Anatomy and Cell Biology, IUSM, Indianapolis, IN, USA.

[6.] Department of Medical and Molecular Genetics, IUSM, Indianapolis, IN, USA.

[7.] Department of Radiology & Imaging Sciences, IUSM, Indianapolis, IN, USA

Corresponding Author: *For correspondence contact Kwangsik Nho, Department of Radiology & Imaging Sciences, IUSM, Indianapolis, IN, USA, Methodist GH4101, RADY, Indianapolis, IN, 46202, USA. Phone: +1-317-963-7503; Email: knho@iupui.edu

Abstract

Alzheimer's disease (AD) is characterized by robust microgliosis and phenotypic changes that accompany disease pathogenesis. Indeed, genetic variants in microglial genes are linked to risk for AD. Phospholipase C γ 2 (PLCG2) participates in the transduction of signals emanating from immune cell-surface receptors that regulate the inflammatory response and is selectively expressed by microglia in the brain. A rare variant in *PLCG2* (P522R) was previously

found to be protective against AD, indicating that *PLCG2* may play a role in AD pathophysiology. Here, we report that a rare missense variant in *PLCG2* confers increased AD risk (p=0.047; OR=1.164 [95% CI=1.002-1.351]). Additionally, we observed that *PLCG2* expression levels are increased in several brain regions of AD patients, correlating with brain amyloid deposition. This provides further evidence that *PLCG2* may play an important role in AD pathophysiology. Together, our findings indicate that *PLCG2* is a potential new therapeutic target for AD.

Introduction

Late-onset Alzheimer's disease (LOAD) is the most common form of AD, with symptoms typically arising after age 65 [1]. Age, sex, and the apolipoprotein ε4 (*APOE* ε4) allele are the three greatest risk factors for LOAD [2-4]. The risk for LOAD doubles every five years after age 65, and over 60% of AD patients are female [2,5]. The mechanisms underlying the development of LOAD are incompletely understood, but recent large-scale genome-wide association studies (GWAS) have identified that more than 30 genetic variants are associated with LOAD [6,7].

Importantly, approximately 40% of the identified genes are immune- and microglia-related, suggesting that microglia are involved in modulating AD pathology [8]. Among these microglia-related genetic factors, a rare variant in *PLCG2* (phospholipase C γ 2), P522R (rs72824905-G), was found to be associated with reduced LOAD risk [9]. PLCG2 is a membrane-associated enzyme that catalyzes the conversion of phospholipid PIP2 (1-phosphatidyl-1D-myo-inositol 4,5-bisphosphate) to IP3 (1D-myo-inositol 1,4,5-trisphosphate) and DAG (diacylglycerol), which plays a crucial role in cell-surface receptor signal transduction [10]. Specifically, *PLCG2* is necessary for immune cell function and is highly expressed in microglia. Genomic deletions (exon 19, $\triangle$19, or exon 20 through 22, $\triangle$20-22) or somatic mutations (R665W or S707Y) within the regulatory domain of *PLCG2* resulted in constitutive activation and resistance to treatment by inhibition of its upstream activator, BTK (Bruton's tyrosine kinase), in leukemia [11,12]. Interestingly, a missense M28L variant in *PLCG2* that does not alter the

53 constitutive activity of the enzyme following Rac2 GTPase stimulation has been identified in
54 BTK-inhibitor-resistant patients [13]. BTK inhibition reduces phagocytosis and inhibits the uptake
55 of synaptic structures in rodent microglia, indicating a role for the BTK-PLCG2 pathway in
56 microglial function [14].

57 Here, we report that expression levels of *PLCG2* are increased in AD, and that the M28L
58 variant is associated with elevated LOAD risk. Similarly, *Plcg2* is highly expressed in the brain of
59 an AD mouse model. Importantly, upregulated expression of *PLCG2* is associated with
60 increased amyloid plaques, which was validated in an amyloid mouse model. Elucidating the
61 different effects of *PLCG2* variants on LOAD risk will expand our understanding of the function
62 of microglia in AD pathophysiology.

63 **Results**

64 **The *PLCG2* M28L Variant Confers a Higher Risk for LOAD.**

65 Using previously published large-scale GWAS summary statistics [6], we identified that the
66 missense variant M28L in *PLCG2* is associated with LOAD. The minor allele (T) of M28L in
67 *PLCG2* significantly increased risk for LOAD (p=0.047, OR=1.164 [95% CI=1.002-1.351])
68 (**Table 1**). PLCG2 possesses a set of core domains common to most other isoforms of PLC,
69 including an N-terminal PH domain, two pairs of EF hands, a catalytic TIM barrel composed of
70 the X- and Y-boxes, and a C2 domain (**Fig. 1a)**. The PLCG isozymes elaborate on this core with
71 a unique array of regulatory domains, including a split PH (sPH) domain, two SH2 domains, and
72 an SH3 domain. Two substitutions that modulate risk for LOAD, M28L, and P522R, were
73 mapped onto a protein structure homology model of PLCG2 [15] (**Fig. 1b**). M28 is buried in the
74 core of the PH domain but is not visible in a space-filling model (**Fig. 1c**). The PH domain is
75 essential for membrane association of PLCG2.

76 ***PLCG2* Expression Levels are Increased in LOAD.**

77 We performed gene expression analysis using RNA-Seq data generated from seven
78 brain regions. The demographic information of the participants included in this study is

summarized in **Table 2**. We found that *PLCG2* was over-expressed in LOAD in the temporal cortex (logFC=0.27, p=4.56E-02; **Fig. 2a**), parahippocampal gyrus (logFC=0.55, p=1.74E-03; **Fig. 2b**), superior temporal gyrus (logFC=0.46, p=2.55E-02; **Fig. 2c**), and inferior prefrontal gyrus (logFC=0.36, p=1.38E-02; **Fig 2d**) with age and sex as covariates (**Table 3**). However, we did not find any diagnosis group differences in the cerebellum (**Fig. 2e**), frontal pole (**Fig. 2f**), and dorsolateral prefrontal cortex (**Fig. 2g**) (**Table 3**). With age, sex, and *APOE* ε4 carrier status as covariates, *PLCG2* remained over-expressed in LOAD in the parahippocampal gyrus (logFC=0.57, p=2.02E-03), superior temporal gyrus (logFC=0.42, p=4.95E-02), and inferior prefrontal cortex (logFC=0.33, p=2.60E-02) (**Table 3**). In the parahippocampal gyrus, superior temporal gyrus, and inferior prefrontal gyrus, *PLCG2* was over-expressed in LOAD with and without *APOE* ε4 carrier status as an additional covariate. We investigated whether *PLCG2* expression levels were associated with expression levels of microglia-specific marker genes (*AIF1* and *TMEM119*). Our analysis revealed that expression levels of *AIF1* and *TMEM119* were significantly associated with *PLCG2* expression levels in the frontal pole (*AIF1*: β=0.258, p=1.09E-06; *TMEM119*: β=0.518, p=1.28E-15), superior temporal gyrus (*AIF1*: β=0.33, p=8.98E-07; *TMEM119*: β=0.71, p<2E-16), parahippocampal gyrus (*AIF1*: β=0.419, p=5.43E-07; *TMEM119*: β=0.806, p<2E-16), and inferior prefrontal gyrus (*AIF1*: β=0.257, p=6.15E-06; *TMEM119*: β=0.582, p=6.64E-15) (**Table 4**).

Increased *PLCG2* Expression Levels are Associated with Amyloid Plaque Density in the Human Brain.

We performed an association analysis of *PLCG2* expression levels with mean amyloid plaque densities measured in four brain regions. Expression levels of *PLCG2* in the human brain was associated with amyloid plaques in three brain regions (**Table 4**). Increased *PLCG2* expression was associated with increased amyloid plaques in the parahippocampal gyrus (β=0.027, p=5.22E-05; **Fig. 3a**), superior temporal gyrus (β=0.026, p=2.02E-04; **Fig. 3b**), and

inferior prefrontal cortex (β=0.017, p=2.73E-03; **Fig. 3c**), but not in the frontal pole (β=0.01, p=0.08; **Fig. 3d**).

PLCG2 Expression Levels are Increased in a Mouse Model of Amyloid Pathology.

Plcg2 expression was increased in a mouse model of amyloid pathology, which is in accordance with the results from our analysis of human LOAD. In the 5xFAD mice, *Plcg2* expression was increased in the cortex (**Fig. 4a**) and hippocampus (**Fig. 4b)** of four-, six -and eight-month-old mice (4-month: 1.39-fold in the cortex, 1.37-fold in the hippocampus; 6-month: 2.37-fold in the cortex, 1.96-fold in the hippocampus; and 8-month: 2.43-fold in the cortex and 2.67-fold in the hippocampus) (**Fig. 4**). Furthermore, our analysis showed a disease progression-dependent increase in *Plcg2* expression in mice with amyloid pathology (**Fig. 4**).

Common Single Nucleotide Polymorphisms in _PLCG2_ are Associated with _PLCG2_ Expression Levels.

We performed an expression quantitative trait loci analysis (eQTL) analysis of *PLCG2* expression levels using common SNPs, including ±20kb from the gene boundary; minor allele frequency (MAF) > 5%, from whole-genome sequencing. The eQTL analysis identified several variants that are associated with *PLCG2* expression levels. In particular, rs4420523 was most significantly associated with *PLCG2* expression levels in the superior temporal gyrus (p=2.43E-06, **Fig. 5a**). Individuals with minor alleles of rs4420523 (C) have higher *PLCG2* expression levels compared to those without minor alleles (**Fig. 5b**). The eQTL association of rs4420523 was replicated in the temporal cortex of the MAYO cohort (**Fig. 5c and Fig. 5d**). Furthermore, using the GTEx eQTL database, we found that rs4420523 is significantly associated with *PLCG2* expression levels in several brain regions and other organs (**Fig. 5e**).

Discussion

In this study, we report the first evidence that a missense variant (M28L) in *PLCG2* is associated with increased risk for LOAD. The results indicated that different genetic variants in *PLCG2* may be either advantageous or deleterious in LOAD, suggesting a potentially important

role of this gene in modifying AD risk. The M28L variant was previously found to be associated with leukemia and mechanistically linked to disease pathogenesis by its resistance to inhibition of its upstream kinase activator BTK [13]. PLCG2 activity can be regulated by several mechanisms, including phosphorylation by kinases such as BTK[16,17], PH domain-dependent regulation [18-20], SH2 domain-containing components regulation [21], and autoregulation of the intrinsic inhibition region [21,22]. The methionine 28 is buried within the N-terminal PH domain, and the substitution likely leads to a less well-packed PH domain with a concomitant loss of domain stability. The instability of the PH domain may affect the protein-protein interactions that regulate enzymatic activity. Additionally, the conformational change may disrupt PLCG2-BTK or other protein interactions, leading to ibrutinib resistance. *PLCG2* is selectively expressed by microglia in the brain [23], and the M28L mutation likely induces a dysfunctional microglial phenotype with significant implications in AD pathology. Conversely, the P552R PLCG2 variant has been found to reduce AD risk [9,24-27]. Therefore, determining how the M28L and P522R variants affect enzyme activity and microglial phenotype will provide valuable insights into the role of *PLCG2* in AD. Importantly, further analysis of the *PLCG2* M28L variant using human datasets is limited due to the very low frequency of this variant. Specifically, it was not possible to investigate the interaction of the *PLCG2* M28L variant with *PLCG2* expression, amyloid plaques, and *APOE* ε4. Therefore, larger cohorts are required to confirm our observation and perform a more comprehensive study of the role of the *PLCG2* M28L variant in microglia-mediated AD pathology.

Furthermore, we found that *PLCG2* expression increases in several brain regions of LOAD patients, which correlates with brain amyloid plaque density and expression levels of microglial markers *AIF1* and *TMEM119* [28-30]. These results highlight an important relationship between amyloid plaques and *PLCG2* expression, which is further supported by increased levels of *Plcg2* throughout disease progression in the 5xFAD mice, a well-studied model of amyloid pathology[22]. *PLCG2* expression is also upregulated in the amyloid models TgCRND8

and App $^{NL\text{-}G\text{-}F/NL\text{-}G\text{-}F}$ mice[31]. Interestingly, microglia surrounding cortical plaques in TgCRND8 mice express *Plcg2* [23], further implicating *PLCG2* in microglial response to Aβ. Nonetheless, further studies are necessary to investigate the role of *PLCG2* in plaque-associated microglia.

eQTL analysis was performed to gain insight into the relationship between genetic variants and *PLCG2* expression levels. The SNP most significantly associated with *PLCG2* expression levels was rs4420523, an intronic variant. Within the same haplotype blocks [32], about ten variants that significantly increased *PLCG2* expression were strongly correlated with rs4420523, including a synonymous *PLCG2* variant, rs1143688. Further studies to investigate whether increased gene expression by the *PLCG2* variants is related to AD pathogenesis are of great interest.

In conclusion, we identified a novel association between a missense variant in *PLCG2* (M28L) and an increased risk for LOAD. Additionally, we showed that *PLCG2* expression was increased in several brain regions of LOAD patients and strongly correlated with brain amyloid burden in LOAD patients and AD animal models. Our results provide further evidence that *PLCG2* may play an important role in AD pathophysiology. Future studies investigating how the M28L and P522R variants in *PLCG2* modulate its function and microglia phenotypes in AD could lead to the identification of potential therapeutic strategies focused on PLCG2 activity.

Materials and Methods

Human participants and RNA-Seq

RNA-Seq and whole-genome sequencing data were obtained from the Accelerating Medicines Partnership for Alzheimer's Disease (AMP-AD) Consortium, where all individuals used in the analysis were participants of the Mayo Clinic Brain Bank cohort, the Mount Sinai Medical Center Brain Bank (MSBB) cohort, and the Religious Orders Study and Memory and Aging Project (ROSMAP) cohort.

In the Mayo Clinic RNA-Seq dataset[33], RNA was isolated from the temporal cortex (TCX) and cerebellum (CER). The RNA-Seq-based whole transcriptome data were generated from

human samples of 151 TCX (71 cognitively normal older adult controls (CN) and 80 LOAD) and 151 CER (72 CN and 79 LOAD). LOAD had a Braak score of ≥ 4.0 and met neuropathological criteria for AD, while CN had a Braak score of ≤ 3.0 and without neurodegenerative diagnoses. The quality of the samples was selected to be RNA integrity number (RIN) ≥ 5.0 for inclusion in the study.

In the MSBB dataset[34], RNA was isolated from the top two most vulnerable regions of LOAD, parahippocampal gyrus (PHG) and inferior frontal gyrus (IFG), and the ranked 7th and 14th most vulnerable brain regions of LOAD, superior temporal gyrus (STG) and frontal pole (FP).

The assessment of dementia and cognitive status was conducted using a clinical dementia rating scale (CDR)[35]. LOAD had a CDR score of ≥ 0.5, while mild cognitive impairment (MCI) had a CDR score of 0.5, and CN had a CDR score of 0 without any significant memory concern of their daily activity. This study included 108 participants (16 CN, 14 MCI, and 78 AD) for PHG, 137 participants (21 CN, 18 MCI, and 98 LOAD) for STG, 136 participants (18 CN, 16 MCI, and 102 LOAD) for IFG, and 153 participants (22 CN, 20 MCI, and 111 LOAD) for FP.

In the ROSMAP dataset[36], RNA-Seq was performed on dorsolateral prefrontal cortex from 241 participants (86 CN and 155 LOAD). The diagnosis is based on the assessment of clinical diagnosis of cognitive status, which followed the criteria of the joint working group of the National Institute of Neurological and Communicative Disorders and Stroke and the Alzheimer's Disease and Related Disorders Association.

Whole Genome Sequencing (WGS)

Pre-processed whole-genome sequencing data were obtained from the Accelerating Medicines Partnership for Alzheimer's Disease (AMP-AD) Consortium [33,34,36-38]. Whole-genome sequencing libraries were prepared using the KAPA Hyper Library Preparation Kit per the manufacturer's instructions. Libraries were sequenced on an Illumina HiSeq X sequencer using

pair-end read chemistry and read lengths of 150bp. The paired-end 150bp reads were aligned to the NCBI reference human genome (GRCh37) using the Burrows-Wheeler Aligner (BWA-MEM)[39] and processed using the GATK best practices workflow that marks potential duplicates, locally realigns any suspicious reads, and re-calibrates the base-calling quality scores using Genome Analysis Toolkit (GATK)[40]. The resulting BAM files were analyzed to identify variants using the HaplotypeCaller module of GATK for multi-sample variant callings[41].

Statistical analysis

To investigate the diagnosis group difference of *PLCG2* expression between CN, MCI, and LOAD, we used the *limma* software[42] to perform a differential expression analysis[36]. Age, sex, and *APOE* ε4 carrier status were used as covariates. To investigate the relationship between *PLCG2* expression levels and amyloid plaque density or expression levels of microglia specific markers (*AIF1 and TMEM119)*, we used general linear models with *PLCG2* expression levels as a dependent variable and plaque density or microglia specific markers as well as age, sex, and *APOE* ε4 carrier status as explanatory variables. The regression was performed with the "glm" function from the stats package in R (version 3.6.1).

In the mouse study, statistical analyses were performed using GraphPad Prism (Version 8.4.2). Experiments at the 2-, 4-, 6- and 8-month time points were performed independently, so statistical comparisons between wild-type and 5xFAD AD mice were performed by unpaired t-test. Graphs represent the mean, and error bars denote the SEM.

Mice

All wild-type and 5XFAD mice used in this study were maintained on the C57BL/6J background and purchased from Jackson Laboratory (JAX MMRRC Stock# 034848). All mice were bred and housed in specific-pathogen-free conditions. Both male and female mice were used in this study.

Mouse RNA isolation for qPCR

Mice were anesthetized with Avertin and perfused with ice-cold PBS. The cortical and hippocampal regions from the hemisphere were micro-dissected and stored at -80-degree C. Frozen brain tissue was homogenized in buffer containing 20 mM Tris-HCl (pH=7.4), 250 mM sucrose, 0.5 mM EGTA, 0.5 mM EDTA, RNase-free water, and stored in an equal volume of RNA-Bee (Amsbio, CS-104B) at -80-degree C until proceeding to RNA extraction. RNA was isolated by using chloroform extraction and purified by using the Purelink RNA Mini Kit (Life Technologies). The cDNA was prepared from 750 ng of RNA by using high-capacity of RNA-to-cDNA kit (Applied Biosystems), and the qPCR was performed by using the StepOne Plus Real-Time PCR system (Life Technologies) with Taqman Gene Expression Assay (Mm01242530_m1 from the Life Technologies). The relative gene expression was determined by using $\Delta\Delta$CT and assessed relative to GAPDH (Mm99999915_g1). A Student's t test was performed for qPCR assays, comparing the results of wild-type and 5XFAD animals.

Expression quantitative trait loci (eQTL) analysis

To perform an eQTL analysis of *PLCG2* expression levels, we used common SNPs (±20kb from the gene boundary; minor allele frequency (MAF) > 5%) from whole-genome sequencing. Only non-Hispanic Caucasian participants were selected. In addition, age and sex were used as covariates. The results of the eQTL analysis were plotted with LocusZoom [43].

Homology Modeling

The model of PLCG2 structure containing all residues from amino acid 14-1190 was built by using the template of PLCG1 model [44]. The cartoons with substitutions of M28L and P522R were generated with PyMol (The PyMOL Molecular Graphics System, Version 2.0 Schrödinger, LLC).

Author contributions

A.P.T, J.S, S.J.B, A.L.O, G.W.C, Y.L, G.E.L, B.T.L, and K.N designed the study. A.P.T, C.D, C.P, M.M, P.B.L, N.H, and K.N performed the experiments and analyzed the data. A.P.T,

M.M, G.E.L, and K.N wrote the manuscript. All authors discussed the results and commented on the manuscript.

Acknowledgments

We thank Louise Pay for critical comments on the manuscript and Alison Goate (Icahn School of Medicine), Thomas Wingo (Emory University), and Aliza Wingo (Emory University) for discussion. This work was supported by NIA grant RF1 AG051495 (B.T.L and G.E.L), NIA grant RF1 AG050597 (G.E.L), NIA grant U54 AG054345 (B.T.L et al.), NIA grant R03 AG 063250 (K.N), and NIH grant NLM R01 LM012535 (K.N)

References

1. Isik, A.T. Late onset Alzheimer's disease in older people. *Clin Interv Aging* **5**, 307-11 (2010).
2. Riedel, B.C., Thompson, P.M. & Brinton, R.D. Age, APOE and sex: Triad of risk of Alzheimer's disease. *J Steroid Biochem Mol Biol* **160**, 134-47 (2016).
3. Reiman, E.M. *et al.* Exceptionally low likelihood of Alzheimer's dementia in APOE2 homozygotes from a 5,000-person neuropathological study. *Nat Commun* **11**, 667 (2020).
4. Kim, J., Basak, J.M. & Holtzman, D.M. The role of apolipoprotein E in Alzheimer's disease. *Neuron* **63**, 287-303 (2009).
5. Corrada, M.M., Brookmeyer, R., Paganini-Hill, A., Berlau, D. & Kawas, C.H. Dementia incidence continues to increase with age in the oldest old: the 90+ study. *Ann Neurol* **67**, 114-21 (2010).
6. Kunkle, B.W. *et al.* Genetic meta-analysis of diagnosed Alzheimer's disease identifies new risk loci and implicates Abeta, tau, immunity and lipid processing. *Nat Genet* **51**, 414-430 (2019).
7. Efthymiou, A.G. & Goate, A.M. Late onset Alzheimer's disease genetics implicates microglial pathways in disease risk. *Mol Neurodegener* **12**, 43 (2017).
8. Karch, C.M. & Goate, A.M. Alzheimer's disease risk genes and mechanisms of disease pathogenesis. *Biol Psychiatry* **77**, 43-51 (2015).
9. Sims, R. *et al.* Rare coding variants in PLCG2, ABI3, and TREM2 implicate microglial-mediated innate immunity in Alzheimer's disease. *Nat Genet* **49**, 1373-1384 (2017).
10. Hernandez, D., Egan, S.E., Yulug, I.G. & Fisher, E.M. Mapping the gene that encodes phosphatidylinositol-specific phospholipase C-gamma 2 in the human and the mouse. *Genomics* **23**, 504-7 (1994).

11. Ombrello, M.J. *et al.* Cold urticaria, immunodeficiency, and autoimmunity related to PLCG2 deletions. *N Engl J Med* **366**, 330-8 (2012).

12. Woyach, J.A. *et al.* Resistance mechanisms for the Bruton's tyrosine kinase inhibitor ibrutinib. *N Engl J Med* **370**, 2286-94 (2014).

13. Walliser, C. *et al.* The Phospholipase Cgamma2 Mutants R665W and L845F Identified in Ibrutinib-resistant Chronic Lymphocytic Leukemia Patients Are Hypersensitive to the Rho GTPase Rac2 Protein. *J Biol Chem* **291**, 22136-22148 (2016).

14. Keaney, J., Gasser, J., Gillet, G., Scholz, D. & Kadiu, I. Inhibition of Bruton's Tyrosine Kinase Modulates Microglial Phagocytosis: Therapeutic Implications for Alzheimer's Disease. *J Neuroimmune Pharmacol* **14**, 448-461 (2019).

15. Laskowski, R.A., Stephenson, J.D., Sillitoe, I., Orengo, C.A. & Thornton, J.M. VarSite: Disease variants and protein structure. *Protein Sci* **29**, 111-119 (2020).

16. Hajicek, N., Charpentier, T.H., Rush, J.R., Harden, T.K. & Sondek, J. Autoinhibition and phosphorylation-induced activation of phospholipase C-gamma isozymes. *Biochemistry* **52**, 4810-9 (2013).

17. Peng, Q. *et al.* TREM2- and DAP12-dependent activation of PI3K requires DAP10 and is inhibited by SHIP1. *Sci Signal* **3**, ra38 (2010).

18. Hurley, J.H. & Grobler, J.A. Protein kinase C and phospholipase C: bilayer interactions and regulation. *Curr Opin Struct Biol* **7**, 557-65 (1997).

19. Falasca, M. *et al.* Activation of phospholipase C gamma by PI 3-kinase-induced PH domain-mediated membrane targeting. *EMBO J* **17**, 414-22 (1998).

20. Matsuda, M. *et al.* Real time fluorescence imaging of PLC gamma translocation and its interaction with the epidermal growth factor receptor. *J Cell Biol* **153**, 599-612 (2001).

21. Wang, J., Sohn, H., Sun, G., Milner, J.D. & Pierce, S.K. The autoinhibitory C-terminal SH2 domain of phospholipase C-gamma2 stabilizes B cell receptor signalosome assembly. *Sci Signal* **7**, ra89 (2014).

22. Everett, K.L. *et al.* Characterization of phospholipase C gamma enzymes with gain-of-function mutations. *J Biol Chem* **284**, 23083-93 (2009).

23. Magno, L. *et al.* Alzheimer's disease phospholipase C-gamma-2 (PLCG2) protective variant is a functional hypermorph. *Alzheimers Res Ther* **11**, 16 (2019).

24. van der Lee, S.J. *et al.* A nonsynonymous mutation in PLCG2 reduces the risk of Alzheimer's disease, dementia with Lewy bodies and frontotemporal dementia, and increases the likelihood of longevity. *Acta Neuropathol* **138**, 237-250 (2019).

25. Kleineidam, L. *et al.* PLCG2 protective variant p.P522R modulates tau pathology and disease progression in patients with mild cognitive impairment. *Acta Neuropathol* (2020).

26. Conway, O.J. *et al.* ABI3 and PLCG2 missense variants as risk factors for neurodegenerative diseases in Caucasians and African Americans. *Mol Neurodegener* **13**, 53 (2018).

27. Dalmasso, M.C. *et al.* Transethnic meta-analysis of rare coding variants in PLCG2, ABI3, and TREM2 supports their general contribution to Alzheimer's disease. *Transl Psychiatry* **9**, 55 (2019).

28. Hopperton, K.E., Mohammad, D., Trepanier, M.O., Giuliano, V. & Bazinet, R.P. Markers of microglia in post-mortem brain samples from patients with Alzheimer's disease: a systematic review. *Mol Psychiatry* **23**, 177-198 (2018).

29. Kaiser, T. & Feng, G. Tmem119-EGFP and Tmem119-CreERT2 Transgenic Mice for Labeling and Manipulating Microglia. *eNeuro* **6**(2019).

30. Satoh, J. *et al.* TMEM119 marks a subset of microglia in the human brain. *Neuropathology* **36**, 39-49 (2016).

31. Castillo, E. *et al.* Comparative profiling of cortical gene expression in Alzheimer's disease patients and mouse models demonstrates a link between amyloidosis and neuroinflammation. *Sci Rep* **7**, 17762 (2017).

32. Ward, L.D. & Kellis, M. HaploReg: a resource for exploring chromatin states, conservation, and regulatory motif alterations within sets of genetically linked variants. *Nucleic Acids Res* **40**, D930-4 (2012).

33. Allen, M. *et al.* Human whole genome genotype and transcriptome data for Alzheimer's and other neurodegenerative diseases. *Sci Data* **3**, 160089 (2016).

34. Wang, M. *et al.* The Mount Sinai cohort of large-scale genomic, transcriptomic and proteomic data in Alzheimer's disease. *Sci Data* **5**, 180185 (2018).

35. Morris, J.C. The Clinical Dementia Rating (CDR): current version and scoring rules. *Neurology* **43**, 2412-4 (1993).

36. Bennett, D.A. *et al.* Religious Orders Study and Rush Memory and Aging Project. *J Alzheimers Dis* **64**, S161-S189 (2018).

37. Carrasquillo, M.M. *et al.* Genetic variation in PCDH11X is associated with susceptibility to late-onset Alzheimer's disease. *Nat Genet* **41**, 192-8 (2009).

38. De Jager, P.L. *et al.* A multi-omic atlas of the human frontal cortex for aging and Alzheimer's disease research. *Sci Data* **5**, 180142 (2018).

39. Li, H. & Durbin, R. Fast and accurate long-read alignment with Burrows-Wheeler transform. *Bioinformatics* **26**, 589-95 (2010).

40. DePristo, M.A. *et al.* A framework for variation discovery and genotyping using next-generation DNA sequencing data. *Nat Genet* **43**, 491-8 (2011).

41. Nho, K. *et al.* Comparison of Multi-Sample Variant Calling Methods for Whole Genome Sequencing. *IEEE Int Conf Systems Biol* **2014**, 59-62 (2014).

42. Ritchie, M.E. *et al.* limma powers differential expression analyses for RNA-sequencing and microarray studies. *Nucleic Acids Res* **43**, e47 (2015).

43. Pruim, R.J. *et al.* LocusZoom: regional visualization of genome-wide association scan results. *Bioinformatics* **26**, 2336-7 (2010).

368 44. Hajicek, N. *et al.* Structural basis for the activation of PLC-gamma isozymes by
369 phosphorylation and cancer-associated mutations. *Elife* **8**(2019).

370

Table 1: *PLCG2* M28L confers a higher risk of LOAD

PLCG2 M28L (rs61749044)
p=0.047
OR=1.164 [95% CI=1.002-1.351]

OR *odds ratio*, CI *confidence interval*

Fig. 1 *PLCG2* M28L variant in PH domain

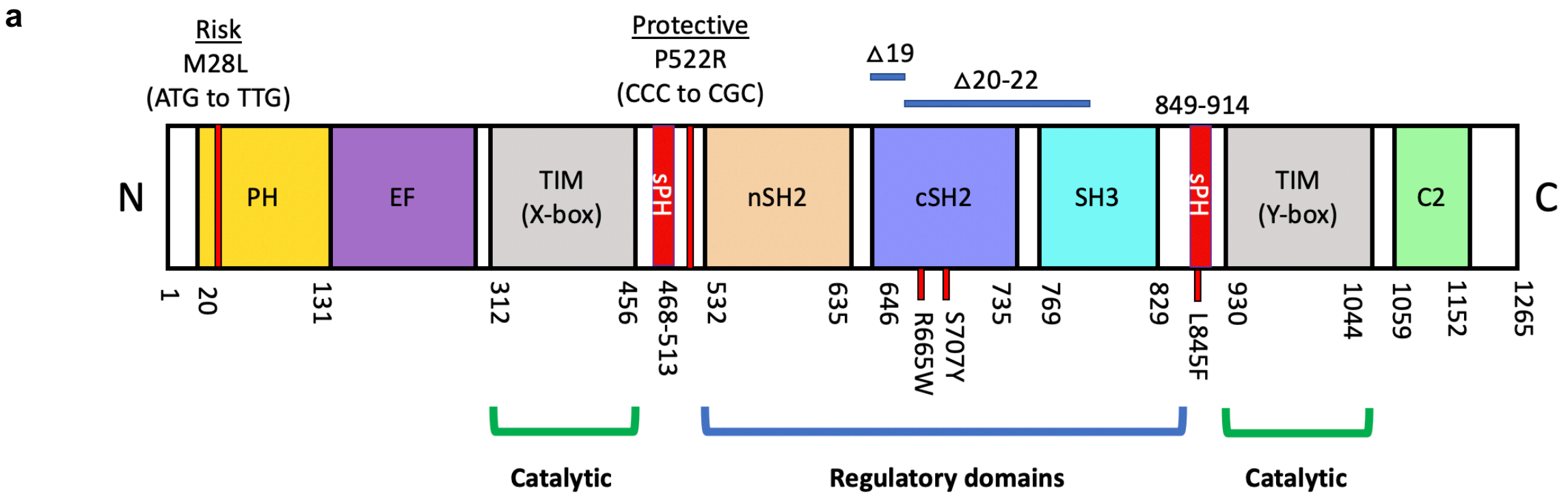

Fig 1. *PLCG2* M28L variant in PH domain.
Domain architecture of *PLCG2* drawn to scale. Genomic deletions (exon 19, Δ19, or exon 20-22, Δ20-22) or somatic mutations (R665W or S707Y) in *PLCG2* within the regulatory domains are shown in the domain architecture. *PLCG2* M28L (risk) and P522R (protective) variants are shown in the domain architecture (a) and mapped onto the structure of PLCG2 (magenta spheres) in both homology model (b) and space-filling model (c).

N *amino-terminus*, C *carboxyl-terminus,* PH *pleckstrin homology domain*, EF *EF hand motif*, TIM *TIM barrel*, sPH *split PH domain*, nSH2 *n-terminus Src Homology 2 domain*, cSH2 *c-terminus Src Homology 2 domain*, SH3 *SRC Homology 3 domain*, C2 *C2 domain*

Fig. 1

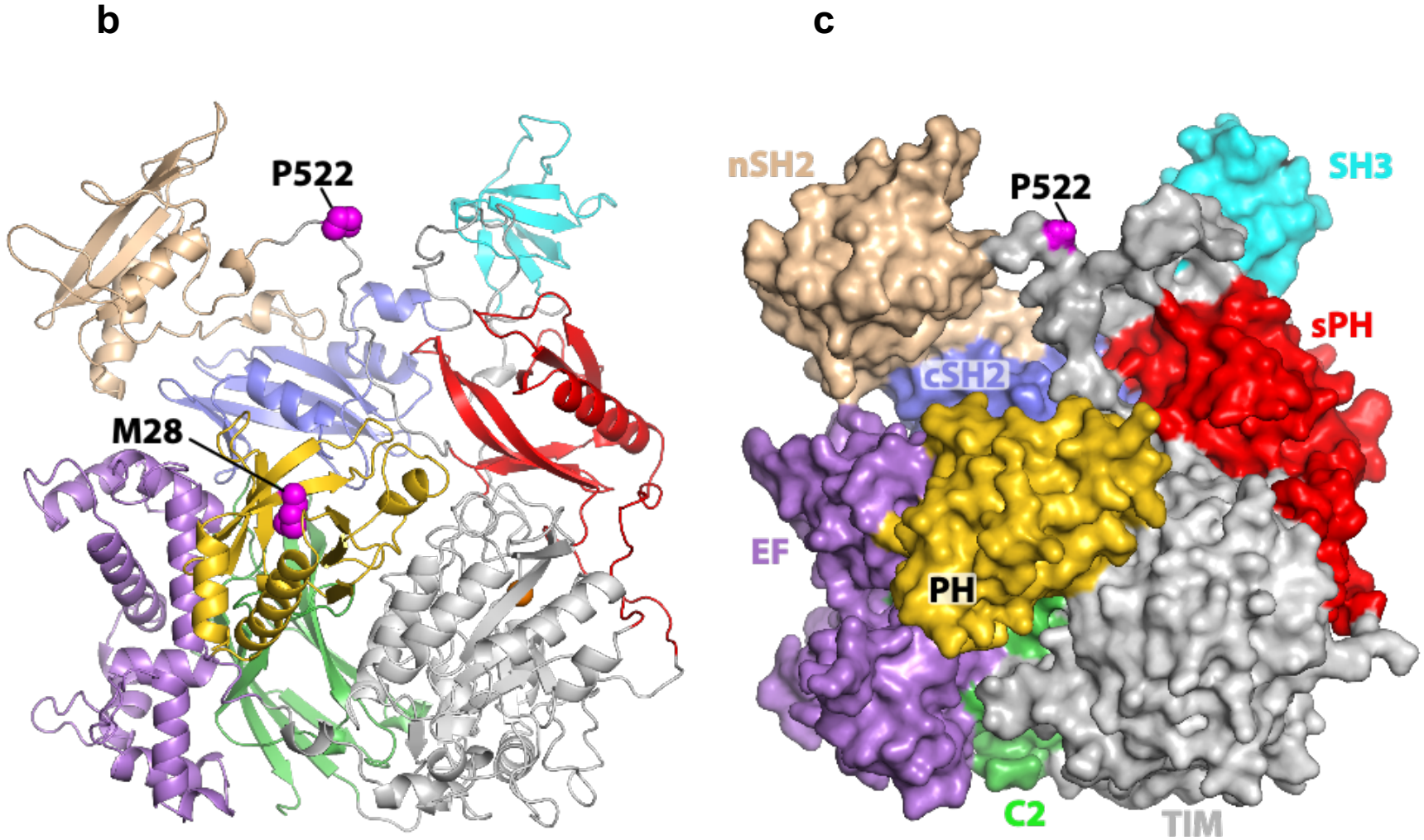

Table 2. Demographic information of the participants included in this study

Brain region	TCX		PHG			STG			IFG			FP			CER		DLPFC	
Diagnosis	CN	AD	CN	MCI	AD	CN	MCI	AD	CN	MCI	AD	CN	MCI	AD	CN	AD	CN	AD
No. of participants	71	80	16	14	78	21	18	98	18	16	102	22	20	111	72	79	86	155
Sex (Female/Male)	35/36	49/31	11/5	7/7	54/25	16/5	11/7	65/33	12/6	7/9	69/33	16/6	11/9	75/36	35/37	47/32	47/39	109/46
Mean age at death (SD), years	82.7 (8.5)	82.6 (7.7)	83.5 (8.9)	80.6 (10.8)	85.5 (6.1)	83.8 (8.1)	82.1 (10.4)	84.5 (6.7)	83.2 (8.6)	80.8 (10.5)	85.4 (6.0)	83.1 (7.7)	83.2 (9.8)	85.4 (5.9)	82.3 (8.3)	82.5(7.7)	83.4 (5.9)	88.2 (3.1)
Mean RIN (SD)	7.7 (1.0)	8.6 (0.6)	7.1 (0.9)	6.7 (0.7)	6.5 (0.9)	6.4 (1.0)	6.4 (0.8)	6.3 (0.9)	8.7 (1.4)	8.8 (1.6)	8.0 (1.8)	6.8 (0.9)	7.0 (1.0)	6.8 (0.9)	7.7 (1.0)	8.4 (0.7)	7.3 (1.0)	6.9 (0.9)
APOE genotype (ε4+/ε4-)	62/9	38/42	14/2	9/5	57/21	17/4	12/6	65/33	16/2	8/8	72/30	19/3	13/7	70/41	62/10	38/41	77/9	91/64

TCX temporal cortex, PHG *parahippocampal gyrus*, STG *superior temporal gyrus*, IFG *inferior temporal gyrus*, FP *frontal pole*, CER *cerebellum*, DLPFC *dorsolateral prefrontal cortex,* CN *cognitively normal* , AD *Alzheimer's disease*, MCI *mild cognitive impairment,* RIN *RNA integrity number,* APOE ε4+/- *carriers and non-carriers of the APOE ε4 allele*

Fig 2. Relative quantification of the *PLCG2* expression in the studied participants

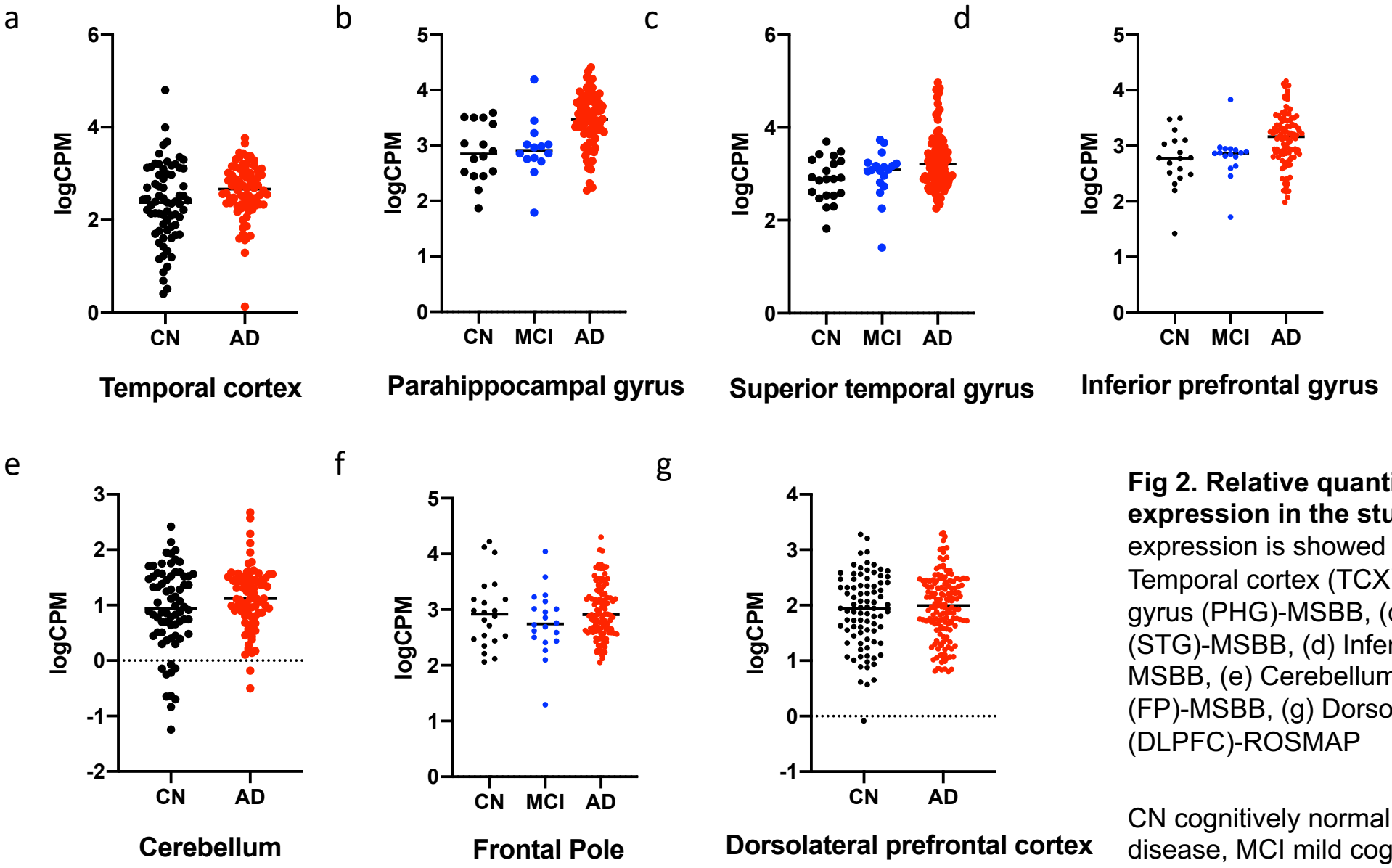

Fig 2. Relative quantification of *PLCG2* expression in the studied participants. Gene expression is showed as logCPM values. (a) Temporal cortex (TCX)-Mayo, (b) Parahippocampal gyrus (PHG)-MSBB, (c) Superior temporal gyrus (STG)-MSBB, (d) Inferior prefrontal gyrus (IFG)-MSBB, (e) Cerebellum (CER)-Mayo, (f) Frontal pole (FP)-MSBB, (g) Dorsolateral prefrontal cortex (DLPFC)-ROSMAP

CN cognitively normal , AD Alzheimer's disease, MCI mild cognitive impairment

Table 3. *PLCG2* expression levels were increased in LOAD

Brain Regions	TCX	PHG			STG			IFG		
Covariate	Age and Sex	Age and Sex			Age and Sex			Age and Sex		
Contrast	CN vs. AD	CN vs. MCI	MCI vs. AD	CN vs. AD	CN vs. MCI	MCI vs. AD	CN vs. AD	CN vs. MCI	MCI vs. AD	CN vs. AD
logFC	0.27056314	0.07196964	0.473066378	0.550085612	0.127793252	0.34416553	0.45549039	0.076802391	0.29211474	0.35622471
p-value	4.56E-02	9.99E-01	6.74E-02	1.74E-03	1.00E+00	1.29E-01	2.55E-02	1.00E+00	5.72E-02	1.38E-02
Covariate	Age, Sex, and *APOE ε4* status	Age, Sex, and *APOE ε4* status			Age, Sex, and *APOE ε4* status			Age, Sex, and *APOE ε4* status		
Contrast	CN vs. AD	CN vs. MCI	MCI vs. AD	CN vs. AD	CN vs. MCI	MCI vs. AD	CN vs. AD	CN vs. MCI	MCI vs. AD	CN vs. AD
logFC	0.248525854	0.02041513	0.492722546	0.569868694	0.097484106	0.329619141	0.415487533	0.007469606	0.300240428	0.33069001
p-value	1.03E-01	1.00E+00	8.71E-02	2.20E-03	1.00E+00	1.73E-01	4.95E-02	1.00E+00	5.96E-02	2.60E-02

Brain Regions	CER	FP			DLPFC
Covariate	Age and Sex	Age and Sex			Age and Sex
Contrast	CN vs. AD	CN vs. MCI	MCI vs. AD	CN vs. AD	CN vs. AD
logFC	0.207937827	-0.188185731	0.178098774	0.02365209	-0.080816649
p-value	9.34E-02	9.85E-01	4.56E-01	9.67E-01	4.53E-01
Covariate	Age, Sex, and *APOE ε4* status	Age, Sex, and *APOE ε4* status			Age, Sex, and *APOE ε4* status
Contrast	CN vs. AD	CN vs. MCI	MCI vs. AD	CN vs. AD	CN vs. AD
logFC	0.2365597	-0.228761625	0.18490708	0.01861041	-0.094639191
p-value	8.46E-02	9.53E-01	4.73E-01	9.82E-01	4.53E-01

Table 3 shows the *p*-value for the gene expression analysis performed by *limma* using RNA-Seq data from AMP-AD Consortium.

TCX temporal cortex, PHG *parahippocampal gyrus*, STG *superior temporal gyrus*, IFG *inferior temporal gyrus*, FP *frontal pole*, CER *cerebellum*, DLPFC *dorsolateral prefrontal cortex,* CN *cognitively normal* , AD *Alzheimer's disease*, MCI *mild cognitive impairment,* logFC *log fold-change*

Table 4. *PLCG2* expression levels were associated with amyloid plaque density and expression levels of microglia specific markers

Brain Regions (MSBB)	Frontal Pole			Parahippocampal Gyrus			Superior Temporal Gyrus			Inferior Frontal Gyrus		
	β	SE	*p*-value	β	SE	*p*-value	β	SE	*p*-value	β	SE	*p*-value
Plaque Mean Density	0.01	0.005	8.45E-02	0.027	0.006	5.22E-05	0.026	0.006	2.02E-04	0.017	0.006	2.73E-03
AIF1	0.258	0.051	1.09E-06	0.419	0.078	5.43E-07	0.33	0.063	8.98E-07	0.257	0.054	6.15E-06
TMEM119	0.518	0.057	1.28E-15	0.806	0.066	<2E-16	0.71	0.064	<2E-16	0.582	0.065	6.64E-15

Table 4 shows the β coefficient (β), standard error (SE), and *p*-value for the association analysis between *PLCG2* expression levels and amyloid plaque density or expression levels of microglia specific markers, *AIF1* and *TMEM119* by general linear models.

Fig 3. Associations of *PLCG2* expression with amyloid plaque mean density

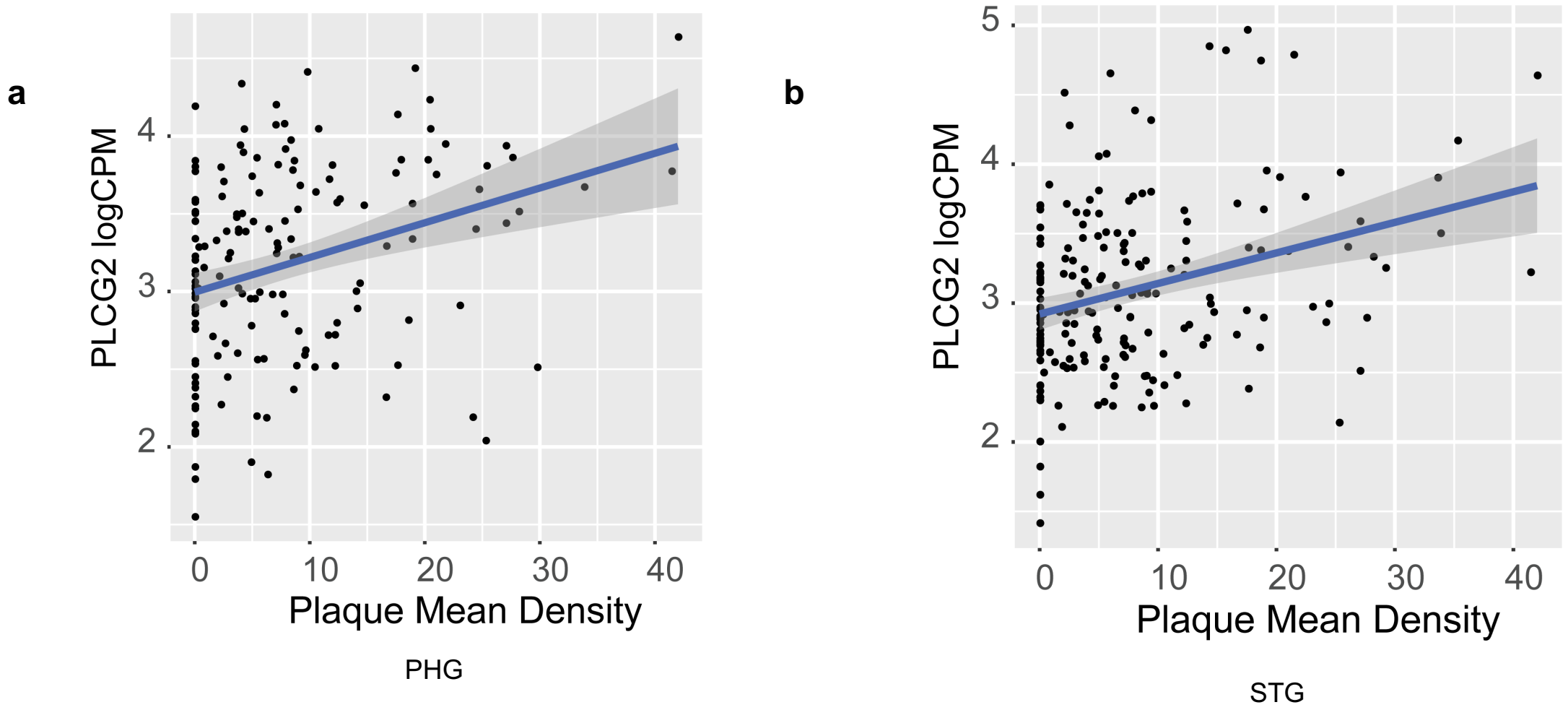

Fig 3. Associations of *PLCG2* expression with amyloid plaque mean density.
The scatter plots show the positive association between *PLCG2* expression and plaque mean density in (a) parahippocampal gyrus, (b) superior temporal gyrus and (c) inferior prefrontal gyrus, and (d) frontal pole from MSBB cohort.

c

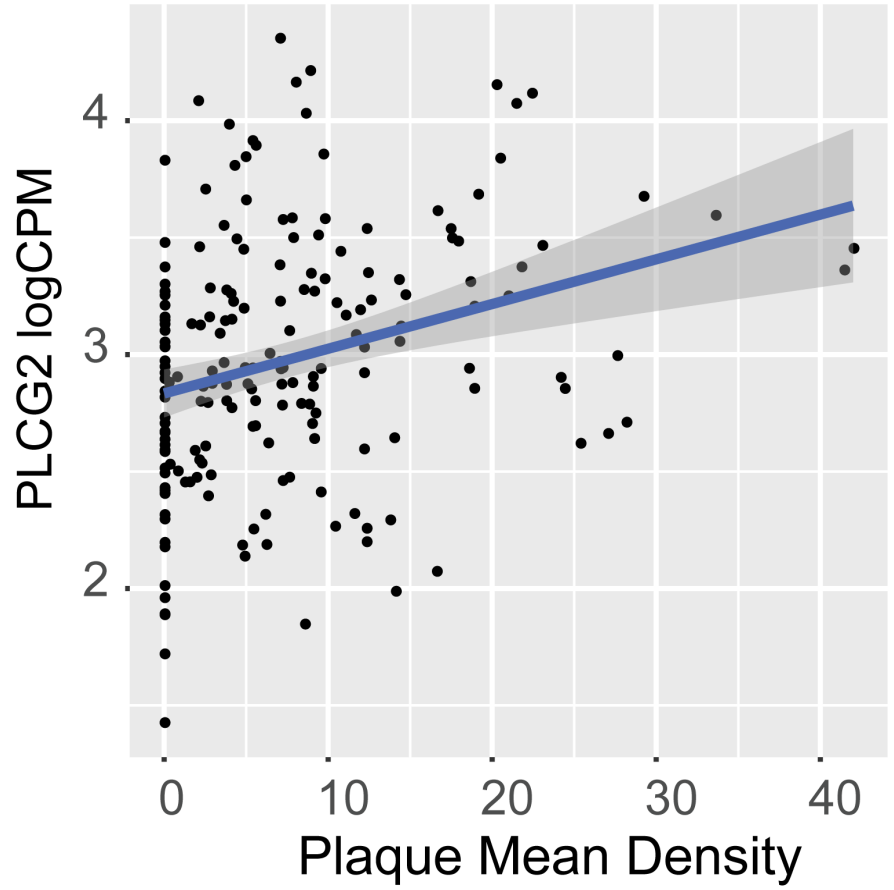
PLCG2 logCPM
4
3
2
0
10
20
30
40
Plaque Mean Density

IFG

d

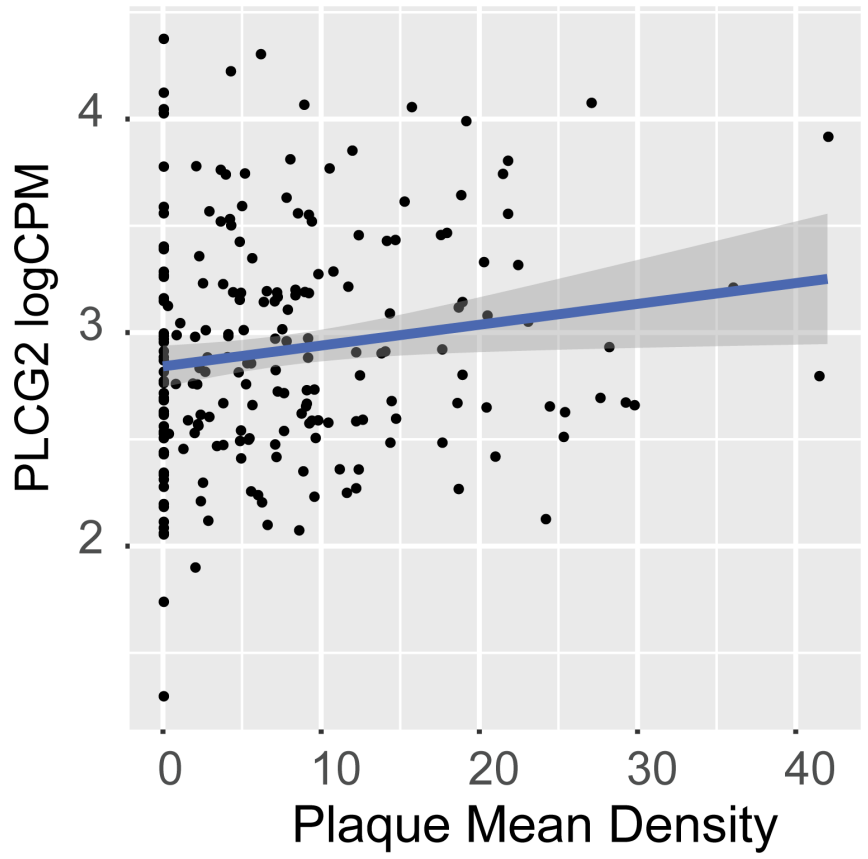
PLCG2 logCPM
4
3
2
0
10
20
30
40
Plaque Mean Density

FP

Fig 4. ***Plcg2* expression levels were increased in a mouse model of amyloid pathology.**

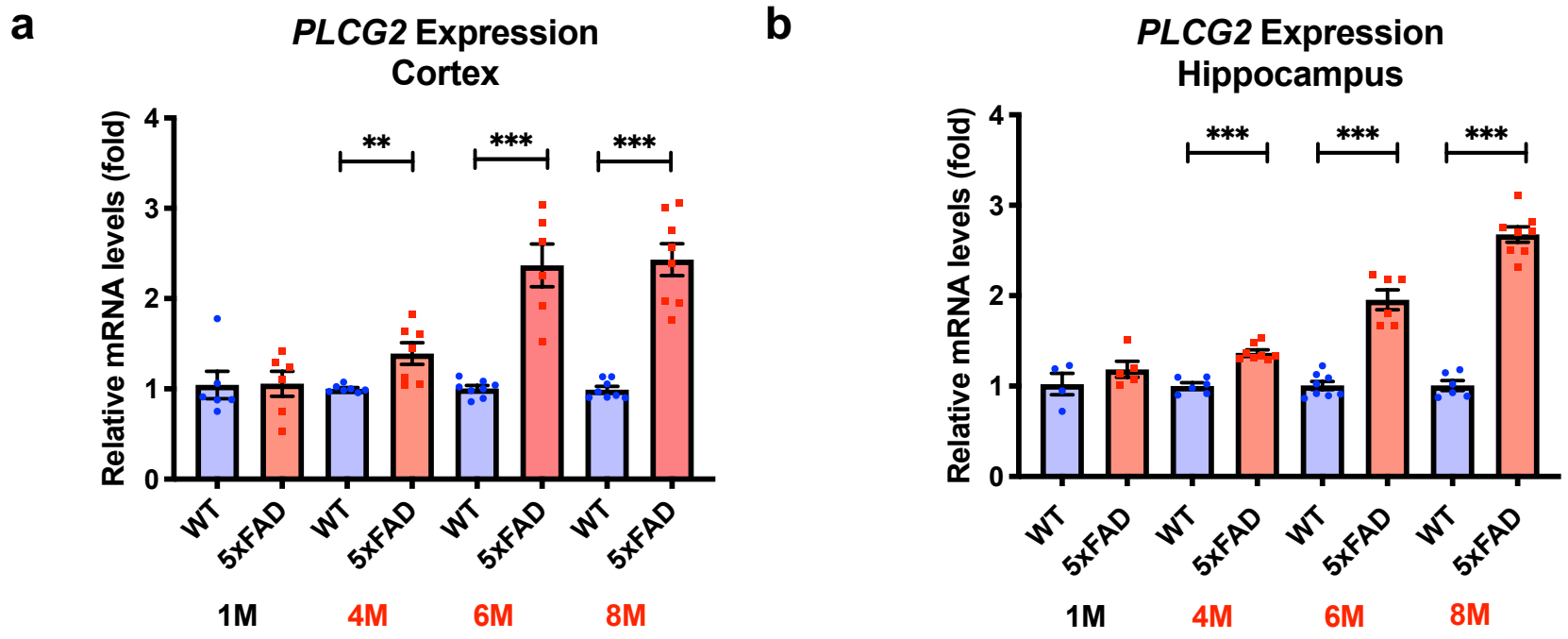

Fig 4. *Plcg2* expression levels were increased in a mouse model of amyloid pathology.
Plcg2 RNA levels were assessed in cortical and hippocampal lysates from 5xFAD mice. There were significant changes in the *PLCG2* gene expression in both cortex (a) and hippocampus (b) at 4 months, 6 months, and 8 months of age (n=4-8 mice). **p<0.01; ***p<0.001

Fig. 5 eQTL analysis of *PLCG2*

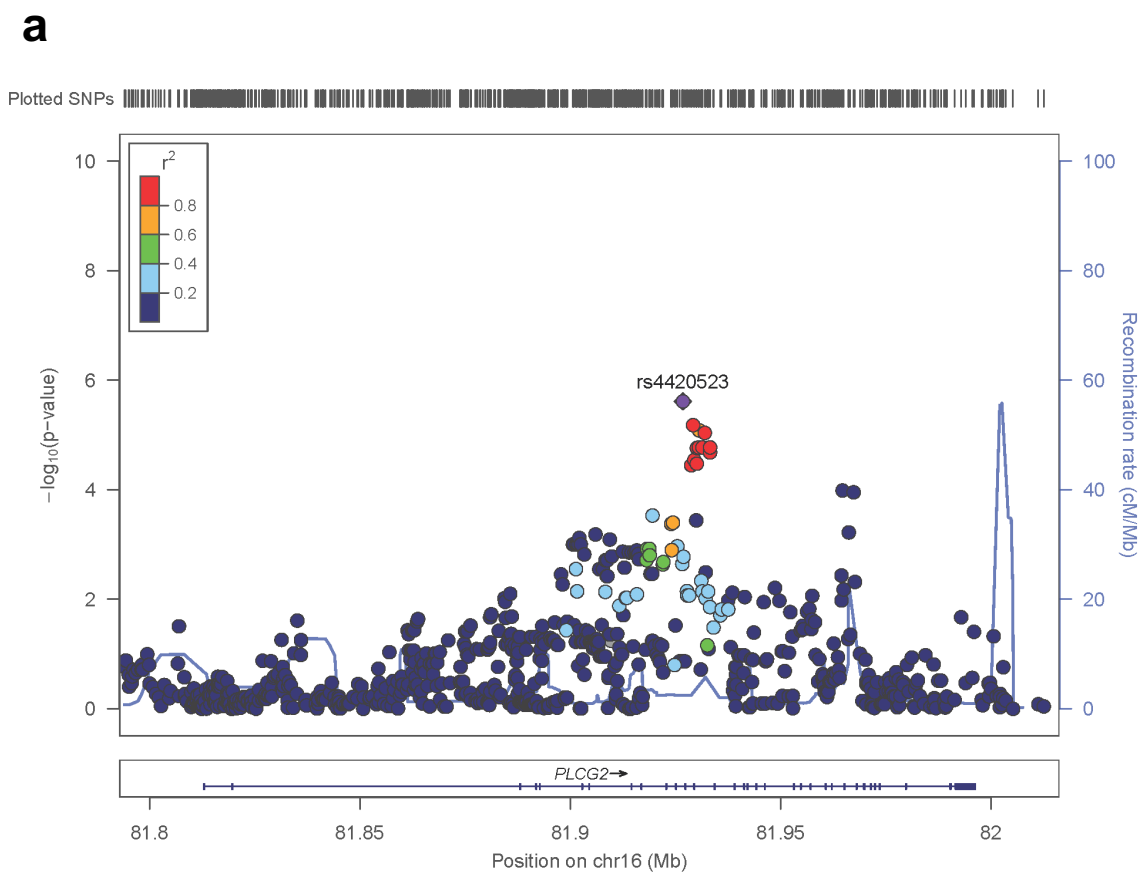

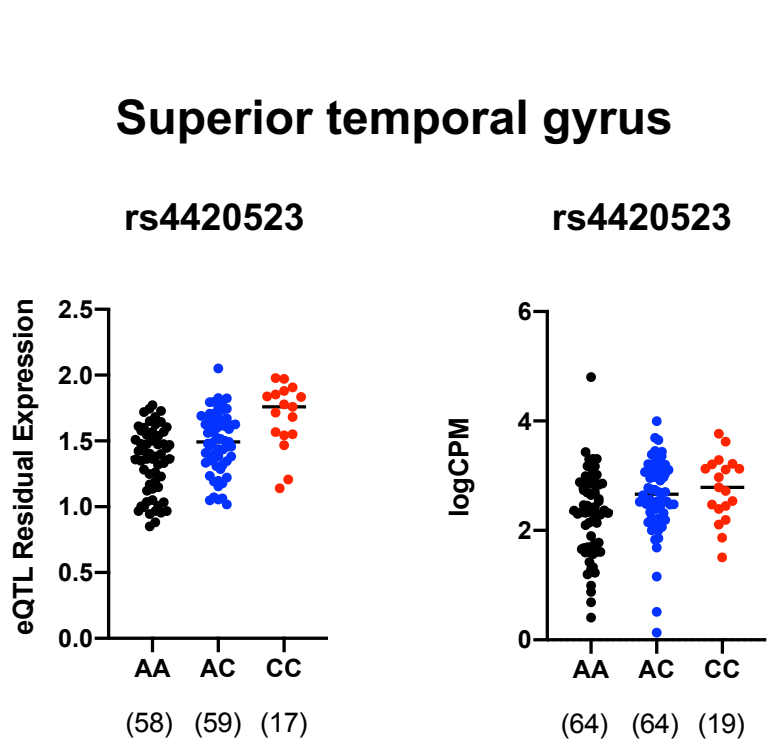

Fig 5. eQTL analysis of *PLCG2*.
SNP positions on chromosome 16 and their color-coded association with *PLCG2* expression from (a) superior temporal gyrus and (c) temporal cortex are plotted by LocusZoom. The SNP (rs4420523) with lowest *p*-value is indicated. The *PLCG2* expression levels of participants with or without rs4420523 are showed as both eQTL residual expression and logCPM value from superior temporal gyrus (b) and temporal cortex (d). The numbers of participants are shown below the genotypes. The results of single-tissue eQTL analysis for rs4420523 are presented in (e).

NES *normalized effect size,* chr16 *chromosome 16,* eQTL *expression quantitative trait loci analysis,* Major allele *A,* Minor allele *C*

c

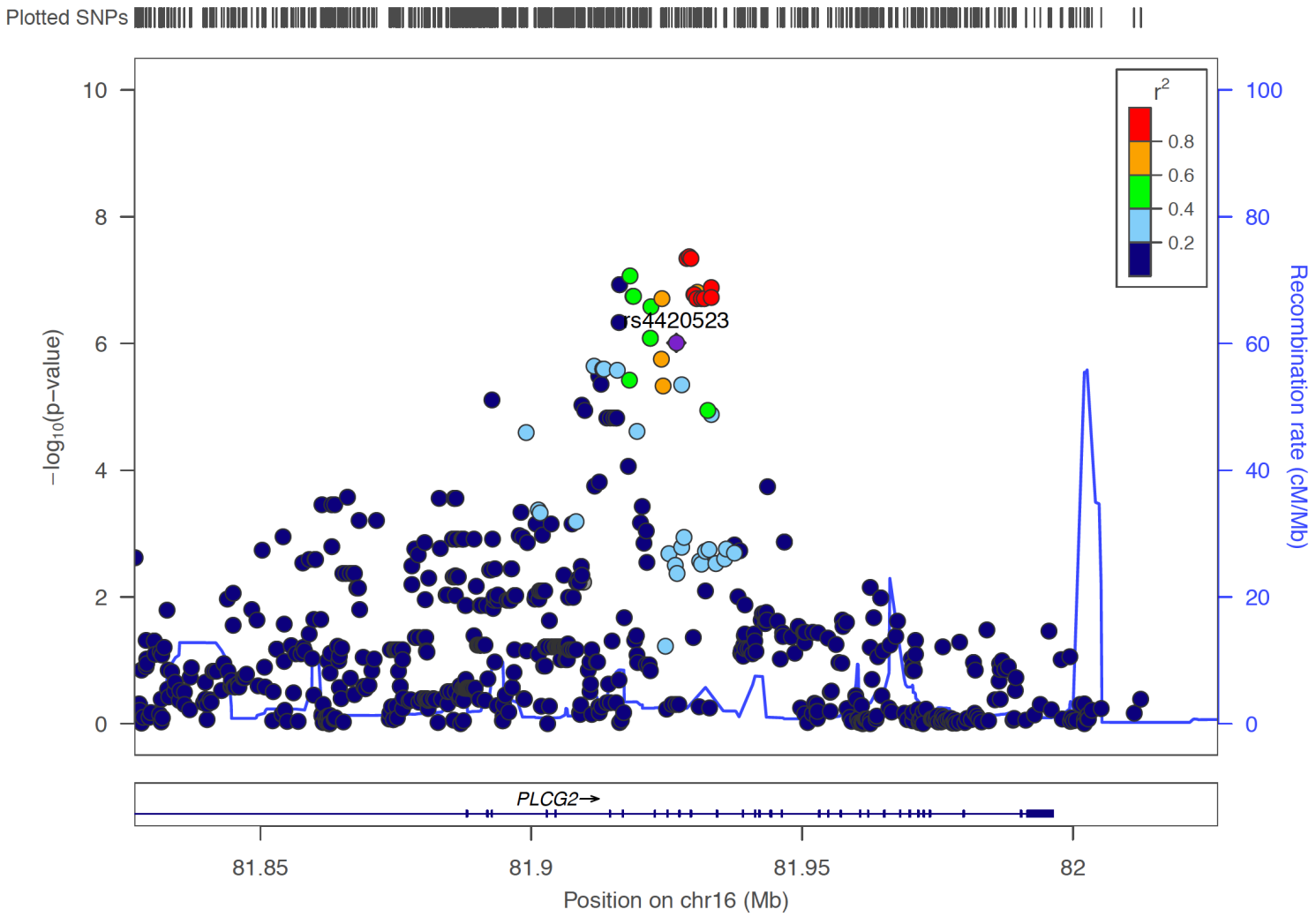
Plotted SNPs
rs4420523
r²
0.8
0.6
0.4
0.2
−log10(p−value)
Recombination rate (cM/Mb)
PLCG2
81.85
81.9
81.95
82
Position on chr16 (Mb)

d

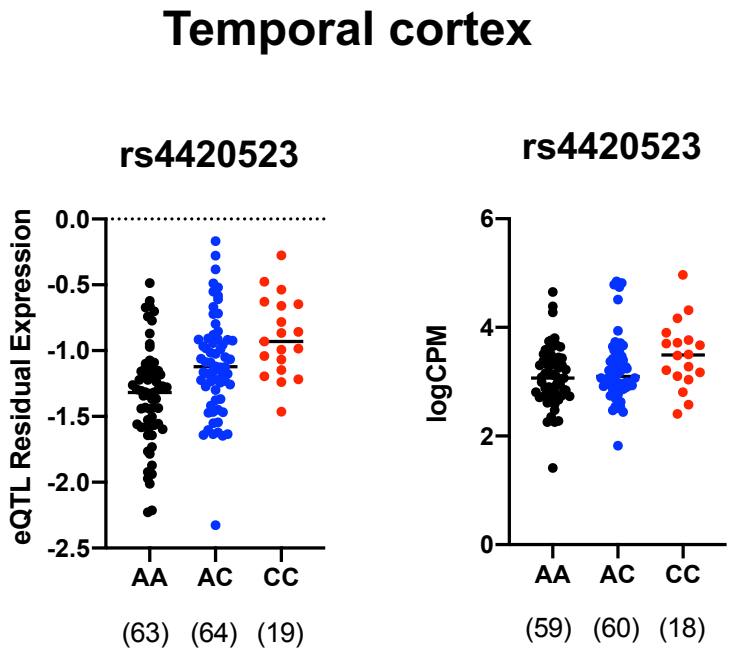
Temporal cortex
rs4420523
eQTL Residual Expression
AA
AC
CC
(63)
(64)
(19)
rs4420523
logCPM
AA
AC
CC
(59)
(60)
(18)

e

Tissue	Samples	NES	p-value	m-value
Brain - Hippocampus	165	0.384	1.1e-9	1.00
Brain - Amygdala	129	0.308	4.3e-8	1.00
Brain - Nucleus accumbens (basal ganglia)	202	0.279	6.2e-6	1.00
Brain - Anterior cingulate cortex (BA24)	147	0.256	1.7e-4	1.00
Brain - Cortex	205	0.246	1.3e-5	1.00
Brain - Cerebellum	209	0.242	1.2e-4	0.998
Brain - Frontal Cortex (BA9)	175	0.234	4.0e-6	1.00
Skin - Sun Exposed (Lower leg)	605	0.180	4.7e-7	1.00
Brain - Substantia nigra	114	0.168	0.02	0.896
Brain - Caudate (basal ganglia)	194	0.163	0.1	0.742
Pancreas	305	0.162	0.02	0.847
Heart - Atrial Appendage	372	0.161	2.3e-3	1.00
Brain - Hypothalamus	170	0.157	1.7e-3	0.998
Stomach	324	0.147	1.3e-4	1.00
Skin - Not Sun Exposed (Suprapubic)	517	0.147	6.7e-5	1.00
Brain - Putamen (basal ganglia)	170	0.139	0.2	0.601
Adipose - Visceral (Omentum)	469	0.120	2.7e-3	1.00
Brain - Spinal cord (cervical c-1)	126	0.117	0.02	0.945
Cells - Cultured fibroblasts	483	0.116	0.03	0.878
Lung	515	0.0985	4.6e-3	0.912
Brain - Cerebellar Hemisphere	175	0.0905	0.2	0.548
Thyroid	574	0.0865	0.007	0.786
Esophagus - Mucosa	497	0.0856	0.02	0.756
Spleen	227	0.0787	0.04	0.496
Breast - Mammary Tissue	396	0.0776	0.03	0.481
Muscle - Skeletal	706	0.0768	0.02	0.462
Esophagus - Muscularis	465	0.0732	0.02	0.462
Nerve - Tibial	532	0.0500	0.2	0.0610
Adipose - Subcutaneous	581	0.0457	0.2	0.0190
Esophagus - Gastroesophageal Junction	330	0.0436	0.2	0.0540
Colon - Transverse	368	0.0234	0.4	0.00500
Liver	208	0.0220	0.7	0.101
Ovary	167	0.0197	0.7	0.0390
Testis	322	0.0145	0.8	0.0770
Whole Blood	670	0.0144	0.4	0.00
Artery - Aorta	387	0.00909	0.7	0.00200
Heart - Left Ventricle	386	-0.00175	1	0.00
Prostate	221	-0.00419	0.9	0.0480
Artery - Coronary	213	-0.0103	0.8	0.00
Colon - Sigmoid	318	-0.0117	0.7	0.00700
Uterus	129	-0.0121	0.9	0.200
Small Intestine - Terminal Ileum	174	-0.0123	0.7	0.00
Pituitary	237	-0.0214	0.7	0.0110
Artery - Tibial	584	-0.0222	0.3	0.00
Cells - EBV-transformed lymphocytes	147	-0.0280	0.7	0.0410
Adrenal Gland	233	-0.0588	0.4	0.0140
Minor Salivary Gland	144	-0.0712	0.4	0.0140
Kidney - Cortex	73	-0.120	0.4	0.198
Vagina	141	-0.149	0.08	0.0510